3D printed chitosan dressing crosslinked with genipin for potential healing of chronic wounds

Forough Hafezi[a], Nikolaos Scoutaris[a], Dennis Douroumis[a], Joshua Boateng[a]*

[a] School of Science, Faculty of Engineering and Science, University of Greenwich at Medway, Central Avenue, Chatham Maritime, Kent ME4 4TB, UK

*Correspondence: Dr Joshua Boateng (J.S.Boateng@gre.ac.uk, joshboat40@gmail.com;

+44 (0) 208 331 8980)

Graphical Abstract

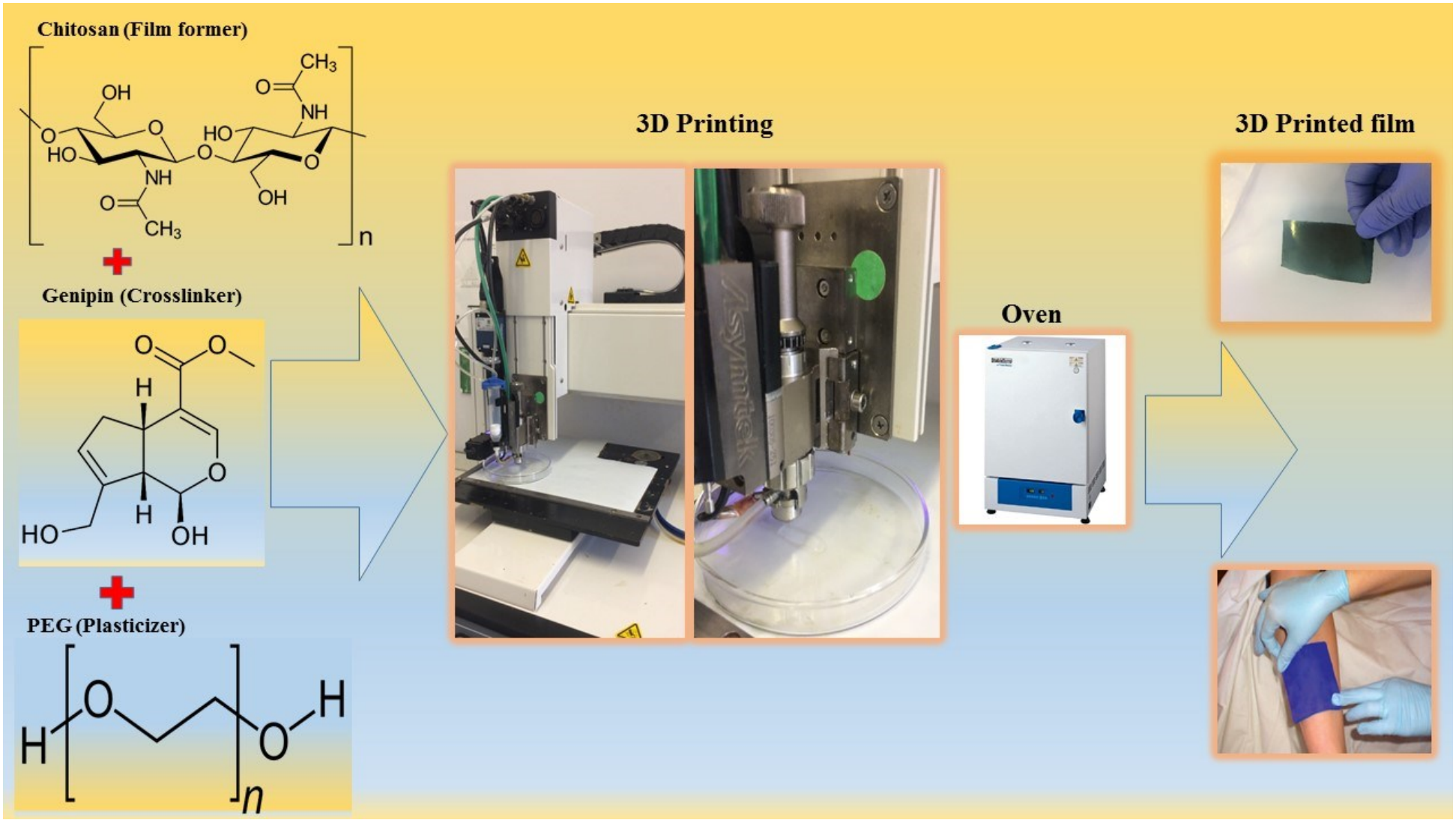

Abstract

Recently, various additive manufacturing (3D printing) approaches have been employed to fabricate dressings such as film scaffolds that possess well defined architecture and orientation at the micro level. In this study, crosslinked chitosan (CH) based film matrices were prepared using 3D printing with genipin (GE) as a crosslinker, with glycerol (GLY) and poly ethylene glycol (PEG) as plasticiser. The 3D printed films were functionally characterized (tensile, fluid handling, mucoadhesion, drug dissolution, morphological properties and cell viability as well physico-chemical characterization using scanning electron microscopy, Fourier transform infrared spectroscopy and X-ray diffraction. CH-GE-PEG600 3D printed films having the ratio of 1:1 polymer: plasticizer was selected due to their appropriate flexibility. Fourier transform infrared results showed intermolecular interaction between CH, GE and PEG which was confirmed by X-ray diffraction showing amorphous matrix structure. *In vitro* mucoadhesion studies of CH-GE-PEG600 films showed the capability of the 3D printed film to adhere to the epithelial surface. Scanning electron microscopy images showed that the surface of the plasticised films were smooth indicating content uniformity of CH, GE and PEG whilst micro cracks in unplasticised films confirmed their brittle nature. Plasticised films also showed high swelling capacity which enhanced water absorption. Cytotoxicity (MTT) assay using human skin fibroblast cell lines demonstrated that more than 90% of cells were viable after 48 hours confirming non-toxic nature of the 3D printed CH-GE-PEG600 films and therefore promising dressing for chronic wound healing applications.

Keywords: 3D printing; Chitosan; Film scaffolds; Genipin; Plasticiser, Tensile testing; Wound healing;

1. Introduction

Skin injuries are common clinical conditions encountered by millions of patients globally and can result in morbidity, disability and as well as possible death, with consequent negative effects on patients' social and economic lives (Singer and Clark, 1999)(Fan et al., 2011)(Schreml et al., 2010). The restoration of skin integrity following an injury remains an important consideration in medical practice including settings such as major surgeries and accident and emergency wards (Jones and Nelson, 2007). In the past, the main concern of wound therapy was to keep the wound bed dry to avoid infection, however, the main objective in current wound management is the maintenance of a balanced moist wound setting which allows the wound to heal in a normal manner (Bowler et al., 2001)(Boateng et al., 2008). The principle is that a moisture-rich environment helps to promote migration of keratinocytes through reinforcing cell movements (Larjava et al., 1993), which ultimately aids in rapid wound healing.

Wound treatment involves both surgical and non-surgical approaches, with dressings being the most commonly employed. The modern dressing approach is to facilitate the wound healing process rather than just covering the wound (Morgan, 2002)(Dhivya et al., 2015). Therefore common dressings including gauze and plasters have largely been replaced with more novel dressings (e.g. films, foams, hydrogels, hydrocolloids) which promote healing via controlling wound exudate in a balanced way to prevent its accumulation in the wound bed, and simultaneously ensuring the availability of an appropriate amount of moisture, which increases the likelihood of optimum skin tissue regeneration with minimum scar formation (Cutting, 2010)(Bhargavi and Kumar, 2011)(Sussman, 2010).

Dressings such as films are used to treat wounds directly and can also be used to deliver drugs such as antimicrobials and anti-inflammatories directly to the wound site, to tackle infections and / or pain (Pawar et al., 2013)(Boateng and Catanzano, 2015). Films are generally

biocompatible and biodegradable and they facilitate application around difficult areas such as joints (knees, ankles and elbows) owing to their flexibility mechanical behaviour (Wittaya-Areekul and Prahsarn, 2006). When applied over the wound, films can also reduce excessive production of wound exudate as well as development and progression of infection in the wound bed (Ehrenreich and Ruszczak, 2006)(Lee and Mooney, 2012). Furthermore, because films are transparent, they allow easy observation of the wound bed without the need for removal, which makes them useful for improving patient compliance because of reduced frequency of dressing changes.

There are various approaches available for the preparation of polymeric films including spray coating, solvent casting and 3D printing. In spray coating, droplets of a molten coating material are dispersed by spraying over an appropriate surface, to produce a uniform film. (Meng et al., 2017)(Pham et al., 2010). Solvent casting involves drying of a polymeric solution or gel in a suitable casting container such as Petri dish or plate. Solvent casting is widely used owing to the ease of manufacturing and cheaper processing costs (Nunes et al., 2016). However, spray coating and solvent casting generally do not have control over functional characteristics which affect dressing performance such as porosity and how the pores interconnect with each other, as well as the structural geometry.

Additive manufacturing techniques (such as 3D printing) have been employed to fabricate scaffolds (films) as potential dressings, possessing well defined architecture and physical orientation (Hafezi et al, 2016). 3D printing typically involves printing of appropriate ‘inks’ (polymer solutions and bioactive gels) to design biocompatible film scaffolds as an advanced alternative to the commonly used solvent evaporated films. The micro-structures of the printed films aid material exchange, cell attachment and migration which allow better tissue regeneration after injury (Dean et al., 2007)(Liu et al., 2016). Furthermore, compared with other methods of fabricating scaffolds (films) (Tong et al., 2016), 3D printing facilitates the

production of more flexible matrices, possessing pre-determined pore sizes, in a reproducible manner, since 3D architectures can be designed using CAD software and printed with the help of fully automated 3D printing facilities (Murphy and Atala, 2014)(Blaeser et al., 2013)(Y. Zhang et al., 2013).

Leong and co-workers identified ideal physical characteristics of 3D printed films capable of facilitating healthy and optimal tissue regeneration (Leong et al., 2003). Their investigation involved use of solid freeform, which has potential to overcome the limitations of spray coating and solvent casting and showed that solid freeform designed films satisfied most of the macro- and micro-architectural characteristics required for tissue engineering in a biomedical setting. Liu and colleagues investigated the effect of 3D bio-printed matrices based on sodium alginate and gelatine when applied on full-thickness wounds in an in vivo mice model and also observed the histopathological changes that occurred over the course of the wound healing progression (Liu et al., 2016). The therapeutic 3D bio-printed matrix consisted a gelatine-alginate grid formed of layers with regular sized pores. The authors reported an average healing time of 16 ± 1 days for the untreated mice and 14 ± 1 days for the animals treated with the 3D printed dressing. Furthermore, histological observations under a microscope confirmed better healing performance of the 3D printed scaffold in the treated mice. They concluded that the biologically active gelatin-alginate printed dressing accelerated the healing process by enhancing formation of granulation and scar tissue. Further, Muwaffak and co-workers, produced antimicrobial loaded wound dressings based on polycaprolactone using 3D printing and loaded with different metals (copper, silver and zinc) and characterized them for physical and antimicrobial properties (Muwaffak et al., 2017). The authors showed that the various formulated dressings exhibited a dual release profile with an initial fast release over 24 hours followed by a slower release over the next 48 hours. They concluded that the 3D scanned and 3D printed scaffolds had the potential for used as personalised wound dressings

and this is particularly useful in the area of chronic wounds where the biochemical, physiological and anatomical aetiology can be complex and varies for different patient groups. The current research reports on 3D-printed films comprising chitosan (CH) as film former, genipin (GE) as crosslinker with either glycerol (GLY) or polyethylene glycol 600 (PEG) as plasticizer, as potential bioadhesive dressing for wound healing purposes. GE has generally replaced crosslinkers such as glutaraldehyde due to advantages such as biocompatibility, well defined chemistry and being less cytotoxic than glutaraldehyde (Muzzarelli, 2009)(Chiono et al., 2008). Further, GE is reported to exhibit pharmacological activity including anti-inflammatory and antibacterial effect (Winotapun et al., 2013) and these together with the biocompatibility make GE relevant for wound healing applications.

The resulting optimized films have been characterized by scanning electron microscopy, X-ray diffraction, Fourier transform infrared spectroscopy, tensile testing, mucoadhesion, swelling, drug dissolution profiles as well as cell viability (biocompatibility) via 3-(4,5-dimethylthiazol-2-yl)-2,5-diphenyltetrazolium bromide (MTT) assay.

2.1 Materials

Medium molecular weight CH, >75-85% deacetylated) and low molecular weight CH, >75-85% deacetylated) were obtained from Sigma Aldrich (St. Louis, USA). GE with (98%) was purchased from Linchuan Zhixin Biotechnology Co., Ltd., Linchuan. Poly ethylene glycol (400 and 600 molecular weights), glycerol, glacial acetic acid, fluorescein sodium (FS), MTT reagent [3-(4,5-dimethylthiazol-2-yl)-2,5-diphenyltetrazolium bromide], Triton-X-100 and dimethyl sulfoxide were all purchased from Sigma–Aldrich (Gillingham, UK). Sodium chloride, potassium chloride, disodium phosphate and monopotassium phosphate were all purchased from Fisher Scientific (UK). Dulbecco's Modified Eagles Medium, fetal bovine serum, penicillin, streptomycin and glutamine were all purchased from Gibco (Paisley, UK).

Human fibroblast cells (ATCC® SCRC1041™) were obtained from American Type Culture Collection-ATCC (Manassas, Virginia, USA).

2.2 Methods

2.2.1 Preparation of 3D printed films

Medium molecular weight CH gels at different concentrations (0.5-1% w/v) were initially prepared as part of preliminary formulation development and concentration was set at 0.5% (w/v) because it did not block the jet dispenser's nozzle. In order to use higher concentrations of CH without blocking the nozzle, low molecular weight CH was employed and gels with concentrations between 0.7-1.4 % (w/v) were attempted and eventually, the maximum concentration was set at 1.2 % (w/v) because it did not block the jet dispenser's nozzle. CH powder and plasticiser (GLY or PEG) were dissolved in 0.5% v/v acetic acid and allowed to stand to allow complete removal of bubbles generated during stirring. Subsequently, 5 ml of GE solution (1% w/v) was mixed with the CH solution and stirring continued for a further 30 minutes to allow complete crosslinking between GE and CH. Once a homogeneous mixture was obtained, the gel was poured into a jet dispenser's (583 Dispenser, Nordson-Asymtek, Maastricht, Netherlands) syringe for printing. Once printed, the hydrogels were dried for 24 hours in an oven (30°C). Moreover, 3D printed films having fluorescein sodium (FS) as model drug were fabricated using selected optimised CH gels from preliminary formulation development. The FS loaded gels were prepared as above at concentration of CH [1.2% (w/v)], PEG600 [1.2% (w/v)] and FS 0.1% (w/v). The resulting FS loaded gel was then poured into the jet dispenser's syringe for printing and the printed gels dried in an oven set to 30°C for 24 hours.

2.3 Tensile evaluation

Tensile behaviour of CH-GE films prepared from various CH gel concentrations, plasticized with different concentrations of GLY and PEG were evaluated with a texture analyser (TA HD

plus, Stable Micro Systems, UK). The films (n = 3) were cut into dumb-bell shapes, attached between the instruments tensile grips and stretched at a speed of 2 mm/s till breaking point, using a trigger force of 0.049 N. The tensile properties were calculated from the force-time plots using relevant equations as previously (Boateng et al, 2009).

2.4 X-ray diffraction

The physical form of the printed films and pure starting materials was carried out using X-ray diffractometry instrument (Bruker AXS GmbH, Karlsure, Germany). In the case of the starting materials (CH and GE) the powders were held together using mylar prior to being loaded onto the sample cell. The films were cut into four pieces, stacked on top of each other, placed on the holder and finally on the sample cell. The instrument settings employed were as follows: diffraction angle of 5° to 50° 2θ, step size of 0.04°, voltage of 40 kV, current of 40 mA, using Cu Kα radiation at a wavelength of 1.54060 Å, and scanning speed set at 0.4 s/step, in transmission mode.

2.5 Fourier transform infrared spectroscopy

Spectra of the films were obtained with the help of a Perkin Elmer (Vatrtwo, Massachusetts, USA) Fourier transform infrared spectrophotometer from 450 to 4000 cm^{-1} over 64 scans on average. The Fourier transform infrared spectrometer was equipped with OMINC® software and a diamond universal attenuated total reflection unit. The samples (pure materials and films) were placed on the diamond crystal and force applied with the help of a pressure clamp which ensured proper contact between the samples and crystal. In all cases, background spectra were subtracted prior to analysis to achieve more accurate and reproducible spectral profiles.

2.6 Scanning electron microscopy

The surface morphology of the plasticised and unplasticised 3D fabricated films was evaluated using a Hitachi SU 8030 scanning electron microscope (Hitachi High Technologies, Krefeld, Germany). Small strips of film samples were applied onto aluminium pin-type stubs with the help of double-sided adhesive carbon tape and coated with chromium using a Sputter Coater (Edwards 188 Sputter Coater S1508). Images were captured at various magnifications at an accelerating voltage of 1 kV with the help of *i-scan* 2000 software.

2.7 Mucoadhesion studies

Mucoadhesion behaviour of the films was evaluated with the help of a texture analyser as described above with gelatin (6.67% w/v) allowed to set in a fridge, used as model mucosal substrate. Prior to mucoadhesion testing, 500µl of phosphate buffered saline (PBS) at a pH of 7.4 was spread evenly over the set gelatin in order to equilibrate the gel surface to simulate wound pH. The PBS was prepared by dissolving 8 g of sodium chloride, 0.2 g potassium chloride, 1.44 g disodium phosphate, 0.24 g monopotassium phosphate in 800ml of deionised water the pH was then adjusted to 7.4 ± 0.1 with sodium hydroxide and then volume made up with distilled water to 1 litre (Boateng and Ayensu, 2014). The films were cut into circular pieces with diameter of 35 mm to fit the probe dimensions. Using double sided adhesive tape, the films (n = 3) were attached to the instrument's 35mm diameter adhesive probe and lowered to make contact with the PBS equilibrated gelatin gel. A trigger force of 0.049 N was applied during the testing, with contact time of 60 seconds and the films moved between the probe and mucosa surface at a speed of 0.5 mm/s till films were detached. The total work of adhesion (WOA), peak of adhesion force (PAF) and cohesiveness were calculated using the instrument Exponent 32 software.

2.8 Swelling (fluid handling) capacity

The fluid handling ability of the films were assessed by measuring the swelling index of the films with time in PBS solution (pH 7.4 ± 0.1) at of 37 ± 0.1°C (Winnicka & Szymańska , 2015). CH-GE (unplasticized) and CH-GE-PEG (plasticized) films were used for this study. Films were cut into pieces, each piece (n = 3) was weighed carefully to obtain an accurate weight and immersed in 5 ml of PBS. The weight changes of the swollen films were recorded at regular time intervals until 120 minutes. For each time point, the PBS was removed and the swollen sample wiped gently with filter paper before weighing to allow an accurate weight of the sample to be measured at each time point. The swelling index (capacity) (IS %) was calculated with the equation below:

$$IS = \frac{Ws - Wd}{Wd} \times 100$$

Ws is swollen weight, *Wd* is the initial dry weight

2.9 *In vitro* drug dissolution studies

Before the dissolution studies, FS content within the film was analysed. The FS loaded film (n = 3) was weighed accurately to 25mg and hydrated in 10 ml of 0.5% (v/v) acetic acid, sonicated for 1 hour and then continuously stirred at room temperature to allow complete dissolution of the CH. Dissolution studies were performed using glass vials containing 2 ml of PBS (pH 7.4) as dissolution medium at 37°C and continuously stirred (200 rpm). The 3D printed films were cut, accurately weighed (20–40 mg) and placed in the glass vials containing dissolution medium (PBS). Aliquots (1 ml) of the PBS medium was sampled out at 1, 2, 3, 4, 5, 24 and 48 hours using a syringe and replaced with 1 ml fresh medium to ensure fixed volume. The sampled dissolution media were filtered and transferred into HPLC vials and analysed using

HPLC. The calculated cumulative percentage drug release at each time point was plotted against time (n = 3).

2.10 HPLC analysis

The concentration of FS was analysed using an Agilent 1200 HPLC system with a Chemstation® software. A Hichrom H5ODS-3799 column, 5 µm particle size (125 x 4.6 mm) and mobile phase comprising acetonitrile, water and trifluoroacetic acid in the ratio 400:595:5 v/v at a flow rate of 1 ml/min and detection at 254 nm was employed. Injection volume was 20 µl and media were filtered before each sample run. A calibration curve of pure standards with concentration range of 10-50 µg/ml was plotted for FS ($R^2 > 0.99$) and used to calculate drug concentration released at each time point.

2.11 *In vitro* cell viability (MTT) studies

Human skin fibroblast cells (ATCC® SCRC1041™) were stored in liquid nitrogen tank (-180ºC) using dimethyl sulfoxide (200 µl in 2 ml media) as a cryopreservative. The frozen cells were thawed according to the ATCC recommended protocol and Dulbecco's Modified Eagle's Medium (ATCC® 302002™) was used to culture the cells. The cells were incubated in an incubator (37°C, 5% CO_2) with medium changes every other day up to 7 days until 80-80% confluence was reached. Cells were detached by trypsin-EDTA solution based on the recommended ATCC procedure. Before cell seeding, the printed film dressings were sterilized using a flow cabinet (NU-437-300E, NUAIRE) with UV light turned on for about 12 hours and transferred into 96 well plates. Cell suspension for the experiment was prepared at concentration of 1 x 10^5 cells/ml and aliquots (100 µl) transferred into 96-well microtiter plates containing the films. 10 µl of MTT solution prepared in PBS (5 mg/ml) was added to the wells

containing the samples and placed in an incubator over a 4 hour period. After the 4 hours of incubation, the supernatant was siphoned off and then dimethyl sulfoxide (100 µl) was added to the wells for dissolving the blue formazan crystals, formed from the MTT due to the succinate dehydrogenase within the cells' mitochondria. The absorbance of the resulting solution was determined at 492 nm with the help of a Microplate Reader. Further, the films alone were assayed as background controls to rule out contribution of absorbance arising from the pure polymers. The final MTT results were based on the average of three replicates ($n = 3$) for each sample tested. The percentage cell viability was calculated by the following equation:

$$\text{Cell viability (\%)} = \frac{\text{At}-\text{Ab}}{\text{Ac}-\text{Ab}} * 100$$

Where At, Ab and Ac are the absorbance of tested samples, medium only and untreated cells, respectively. In this experiment, the untreated cells and Triton-X-100 (0.01% w/v) treated cells were used as negative (100% viable) and positive controls respectively.

3. Result and discussion

3.1 3D printing of films by jet dispenser

The jet dispenser employed in the current study uses a ball-tip at the end of a pneumatic piston to guide the polymer based ink (CH-GE gel) through the small orifice at the tip of the jet nozzle. The piston is lifted by air pressure, causing the polymer solution to move round the piston to enter the nozzle. The piston is returned to the nozzle tip by pressure in the spring upon removal of the air pressure. Once the ball tip makes contact with the nozzle seat, the fluid is activated which leads to the ejection of droplets from the tip of the jet. Several interacting drops of fluid can be deposited at the same position to achieve a much bigger dot. The approach described above has the capability to deposit several drops, up to one hundred per second (Scoutaris et al., 2016). The size of the droplet is controlled by different parameters including the holes of the nozzle, seat and ball tip size, the pressure of the fluid being printed and stroke length. In

this study, a 400 micron nozzle was selected to enable dispensing of large amounts of the viscous printing gels (inks) with high reproducibility.

CH-GE gels at different concentrations (0.5-1.4% w/v) were initially formulated and the optimum concentration of 1.2% (w/v) was selected because it did not block nozzle of the jet dispenser and resulted in films with optimum mechanical properties among all the formulations prepared. There was a need for a plasticizer due to film's brittleness, however, plasticizer effect on the film performance was quantified using texture analysis as outlined below.

3.2 Texture analysis (TA)

As noted above, one of the most important characteristics of film based dressings include the ability to easily apply to difficult areas such as elbows and hips (Boateng et al., 2009). Generally, biopolymers employed to fabricate wound dressings possess weak mechanical strength and ease of use by patients and carers since which therefore limits their potential for use within a clinical setting (Vieira et al., 2011) and therefore require use of plasticizers. Plasticizers are essential in polymeric films and wound dressings because of their ability to enhance the flexibility of polymers via lowering the glass transition temperature (Karki et al., 2016).

Fig. 1 and Fig. 2 show for tensile profiles (strength, elastic modulus and elongation at break) for CH-GE, CH-GE-GLY (different ratios of CH: GLY) and CH-GE-PEG (different ratios of CH: PEG and different molecular weight grades of PEG (400, 600). Unplasticized CH-GE 3D printed films showed low percentage elongation at break (2.44%) which indicates high brittleness and for that reason not suitable to be applied as a dressing for wound healing applications. Therefore, PEG and GLY were incorporated to improve the flexibility of the 3D printed films. Plasticisers such as GLY and PEG act by interfering with hydrogen bond

interaction between the polymer chains, due to its highly hydrophilic characteristics, and as a result decrease the inter molecular forces. This leads to enlargement of the spaces between the polymer chains which reduces the brittleness and promotes flexibility as well as increase in the thickness of the films (Vieira et al., 2011).

For CH-GE-GLY films, there was an inverse relationship between the concentration of GLY and the tensile strength and elastic modulus and a directly proportional relationship with the elongation at break. Fig. 1 showed that 3D printed films at CH: GLY ratios of 4:1 and 2:1 had a higher elongation at break in comparison with unplasticized CH-GE film. However, such high amount of GLY can result in accumulation of exudate or highly wet conditions which could result in skin maceration around the wound area which is a risk factor, clinically, that could result in complications such as infection and ultimately become chronic (Karbowiak et al., 2006)(Boateng et al., 2009).

In CH-GE-PEG 3D printed films (Fig. 2), a similar relationship between the concentration of PEG and the tensile properties was observed as was the case for GLY. Another study by Tanaka and co-workers confirmed that increasing the concentration of plasticizer resulted in a lower tensile strength value with a corresponding increase in the values for percent elongation (Tanaka et al., 2001).

Suyatma and colleagues (Suyatma et al., 2005) investigated the tensile characteristics of CH films in the presence of plasticiser (PEG and GLY) and showed that plasticization improved the CH film ductility. As shown in Fig. 2, CH-GE-PEG600 3D printed films having the ratio of 1:1 of CH: PEG had the highest value of elongation at break (22.67%) which made them an ideal film with a balance between flexibility and toughness (not sticky) among all the other fabricated 3D printed films and was the formulation of choice for further characterization and drug loading.

3.3 X-ray diffraction (XRD)

Fig. 3 shows the X-ray diffraction patterns of the starting compounds (CH and GE) along with the selected optimised 3D printed films (CH-GE-PEG600). The diffractogram of CH exhibited no high intensity peaks which shows its amorphous structure. On the other hand, GE showed high crystallinity as was expected with sharp high intensity peaks (Fig. 3b). The X-ray diffractograms for CH-GE-PEG600 films showed just one broad peak at 14° and another peak at 20° 2θ attributed to mylar. This suggests the amorphous nature of the films, which indicates that GE is molecularly dispersed within the 3D printed polymer matrix (Desai and Park, 2005) and also shows that GE and CH were successfully crosslinked. Zhang and co reported on how different concentration ratios of GE and silk fibroin: (CH) affected the formation of SF–CH microspheres (Zhang et al., 2013). They investigated the X-ray diffraction patterns of CH, GE, silk fibroin, BSA and CH-GE together and confirmed the amorphous nature of CH as well as the crystalline nature of GE.

3.4 Fourier transform infrared spectroscopy

Fig. 4 shows Fourier transform infrared spectra of the starting materials and 3D printed scaffolds. The spectra of CH showed three characteristic bands at 3370 cm^{-1}, 1659 cm^{-1} and 1575 cm^{-1} attributed to the –OH stretching vibration which is generally due to water molecules, $–NH_2$ from the amide group I (C=O), and amide group II respectively (Lambert et al., 1987). There is an overlap of stretching vibrations from the amine (N-H) functional group at 3289 cm^{-1} (Klein et al., 2016). The spectrum of GE showed three characteristic bands at 989, 1088, and 1622 cm^{-1}, assigned to the C-H ring out-of-plane bend, C-H ring in-plane bend, and C=C double bond ring stretch modes of the core of the molecule, respectively (Arteche et al., 2013). Additionally, the C-O-C asymmetric stretch and the CH_3 bend of the methyl ester was observed at 1300 and 1443 cm^{-1}, respectively. Other researchers reported similar Fourier transform

infrared spectra for CH and GE pure compounds (Azevedo et al., 2006)(Bhattarai et al., 2005)(Delgadillo-Armendariz et al., 2014)(Li et al., 2009).

The crosslinking of CH with GE involves a fast reaction in which the amino group of CH makes a nucleophilic attack at the olefinic C-3 atom of GE resulting in the opening of the dihydropyran ring and ultimately in a tertiary amine derivative of GE linked to a glucosamine unit, being formed (Klein et al., 2016). In addition, a slower reaction involving the generation of an amide takes place via a reaction involving the amino group on CH and ester group (by C-11) of GE (Mi et al., 2001). The amide II band observed at 1550 cm^{-1}, which is characteristic of N–H deformation (Lambert et al., 1987), could be attributed to the formation of secondary amides due to the latter reaction between the ester and hydroxyl groups of GE and the amino groups of CH. Pure PEG showed peaks at 1105, 947, and 817 cm^{-1} (Bhattarai et al., 2005) but for the CH-GE-PEG 3D printed films, the hydroxyl, amino and amide groups of CH shifted slightly (3370 cm^{-1} to 3330 cm^{-1} for hydroxyl, 1659 cm^{-1} to 1650 cm^{-1} for amino group and from 1575 cm^{-1} to 1550 cm^{-1} for amide group) due to crosslinking while their intensities decreased due to grafting of PEG (Klein et al., 2016). In comparison to the peak at 1652 cm^{-1} for the amide I peak, the intensity of amide II peak at 1550 cm^{-1} showed a decrease suggesting that the –NH2 groups of CH were linked with the PEG chains (Kolhe & Kannan, 2003).

3.5 Scanning electron microscopy

Scanning electron microscopy images of unplasticized (CH-GE) and plasticized (CH-GE-PEG600) 3D printed films with different magnifications are shown in Fig. 5. The CH-GE films displayed a smooth surface with a homogeneous and dense structure without appearance of any pores on the film surface. This is a good indication that the GE was homogeneously distributed within the composite 3D printed film scaffolds. However, a few cracks were visible on the surface of unplasticized film which is possibly due to absence of plasticiser (PEG) within the

formulations. It can also be observed that the unplasticised films showed a tightly packed matrix architecture which resulted in micro-cracking observed on the film surface (Liu et al., 2013) which confirmed the previous observations from the tensile results that the unplasticised films were brittle in nature. The plasticized 3D printed films exhibited smooth surfaces with no visible cracks as expected, indicating content uniformity of CH, GE and PEG. This is mainly due to presence of PEG as the plasticizing agent which reduces the tensile strength while significantly increasing the percent elongation. Such flexibility is ideal to reduce the chances of causing further injury to the healing tissue. This is particularly true in the case of orthopaedic wounds, which are susceptible to inflammation and swelling and therefore likely to experience friction between the wound bed and the applied dressing (Ousey et al., 2011) and such friction can cause significant pain to the patient. Similar studies by Vieira and co-workers (Vieira et al., 2011) as well as by Suyatma and co (Suyatma et al., 2005) were performed and similar results were reported.

3.6 Mucoadhesion studies by texture analyser

Fig. 6 shows PAF, cohesiveness and WOA of plasticized and unplasticized 3D printed films after detachment from the PBS equilibrated gelatin surface. The plasticized 3D printed films (CH-GE-PEG600) showed a high PAF of (3.05±0.56) and WOA (1.986±0.17) compared to unplasticized films (CH-GE) which had a PAF of (2.7±0.34) and WOA (1.81±0.2). This could be attributed to the effect of PEG as plasticizer which is in agreement with previously reported studies (Morales and McConville, 2011)(Karki et al., 2016) who reported that the incorporation of a plasticizer enhances the mucoadhesive properties. PEG can function by enhancing adhesion through improvement in the hydrogen bonding interaction between the polymeric chain and the model mucosal chains thereby improving mucoadhesion performance (Yadav et al., 2010) and this can be explained by the diffusion theory of mucoadhesion (Yu et al., 2014).

Moreover, plasticized films hydrate better, which is important during the initial stages of mucoadhesion, with hydration enhancing chain inter penetration between the polymeric chains and those of the model mucosal surface, leading to higher detachment force of the films. The high adhesion of the plasticised films implies they will most likely remain longer when applied on the wound surface and therefore potentially reduce the need for regular changes of applied dressing which causes patient non-compliance as a result of pain experienced during dressing removal.

3.7 Swelling (fluid handling) studies

Swelling studies were performed in order to simulate the ability of the 3D printed film scaffolds to adequately handle wound fluid (exudate), using an in vitro model. It is very important to adequately select the medium prior to the swelling studies. Studies were carried out using PBS at pH 7.4 to mimic wound exudate on the surface of the wound. (Szymańska and Winnicka, 2015). PBS is the most commonly used swelling medium to simulate wounds during testing of dressing behaviour. Fig. 7 shows the swelling profiles of the unplasticized (CH-GE) and (CH-GE-PEG) films with time. The maximum swelling capacity of the CH-GE films was 940±99% which was increased to 985±165% for the corresponding plasticised films (CH-GE-PEG600). It was observed that for both films, swelling increased rapidly within the first 5 minutes while maintaining their structural integrity in PBS. However, the films began to lose their integrity after the 30 minutes after which swelling capacity decreased gradually for both films until a steady state was reached at 80 minutes for CH-GE and 90 minutes for CH-GE-PEG600.

It can be observed from the results that the plasticized films swelled to a higher extent in comparison with the unplasticized films. Plasticizer increases the spaces between the polymeric chains and this permits better ingress of water to occupy these inter chain spaces and hence increases rate of hydration which enhances swelling capacity (Roy and Prabhakar,

2010)(Azevedo et al., 2006). Furthermore, CH-GE-PEG600 exhibited lower levels of crystallinity because of favourable interactions between the constituent starting materials. This results in better diffusion of PBS into the films providing a higher swelling ratio (Liu et al., 2012). Further, the swelling capacity of CH-GE-PEG600 films also increased because of the PEG's hydrophilicity. Liu and colleagues showed that the molecular weight of PEG affected the swelling capacity of CH-GE-PEG films (Liu et al., 2012). The higher the molecular weight, the higher the swelling ratio of CH-GE-PEG film. Their results indicated that films plasticised with low molecular weight PEG exhibited the lowest swelling, because of the higher miscibility with CH which was efficient in protecting the PEG from rapid hydration in PBS. The high ability of CH-GE-PEG films to swell makes them suitable for use as absorbent dressings. This makes them ideal for managing exudate by absorbing and retaining excess wound fluid, preventing it from damaging the newly formed wound tissue and the surrounding healthy skin, whilst at the same time allowing an appropriate amount of moisture within the wound bed to facilitate cell migration and proliferation.

3.8 *In vitro* drug dissolution studies

CH provides several advantages for topical drug delivery including bioadhesion, biocompatibility and non-irritancy and antimicrobial action against certain bacteria (Muzzarelli et al., 2015). The in vitro drug release profile in PBS for CH-GE-PEG600 films loaded with FS is shown in Fig. 8. Almost 67% release was achieved within the first hour and 62.72% after 2 hours. Furthermore, the % release decreased slightly between 5 hours and 24 hours. After 24 hours the % release decreased further to 40.21% at 48 hours suggesting possible FS degradation in the dissolution medium with time. Compounds of intermediate polarity (e.g. doxorubicin and FS) were difficult to entrap because of their solubility in the bilayer and surrounding aqueous media (Niesman et al., 1992). FS was used at this stage of the formulation

development as cheap model soluble drug to help with the design of an optimum 3D printed scaffold able to deliver therapeutic agents directly to a chronic wound site to allow the dressing to take active part in the wound healing process. The in vitro drug dissolution profile matched that observed in the swelling study, with rapid initial hydration of the dressing observed within 15 minutes and resulting in rapid release, within the first hour. This confirms that drug release is dependent on initial swelling of the 3D printed film, followed by diffusion of the FS from the swollen polymeric film and possibly via matrix disintegration into the dissolution medium. The drug release profile differs from results reported by Muwaffak and co-workers, using 3D printed polycaprolactone films, where a dual release profile was observed, with an initial fast release over 24 hours followed by a slower release over the next 48 hours (Muwaffak et al., 2017). In a study by Liu and co-workers, it was shown that CH-GE-PEG films with porous micro structure were able to control the rate at which drug was released from the matrix due to sequential dissolution of PEG (Liu et al., 2012). This is because when the water soluble PEG dissolves it results in formation of pores in the structure which accelerate the release of the drug from the swollen film that remains. On the other hand, it has been reported that crosslinking can prolong the duration of the release over a longer period. This is because the addition of GE (crosslinker) to the matrix resulted in hydrogel formation possessing a permanent network structure, due to formation of irreversible chemical links which delays rapid erosion via disintegration and ensures slower drug release due to slower rate of diffusion through the structured matrix.

In an ideal drug delivery dressing, the release of drug over a longer period of 24 to 48 hours is generally helpful for the patient as it avoids the need to remove the dressing frequently. However, Fig. 8 shows that the CH-GE-PEG films did not control the release of the drug compared to the reported studies described above. This is because in this study, we used a highly soluble fluorescent dye which dissolves and diffuses very rapidly from the swollen

dressing matrix and therefore further formulation development will be required in the future using active ingredients with intermediate to low solubility, which will be expected to afford more controlled drug release. Nevertheless, the number of the times that a dressing needs changing is affected by other factors including type of the wound, its size, the amount of the exudate and depth of the wound (Boateng et al., 2008).

3.9 MTT studies

MTT was used to evaluate the effect of the optimized CH-GE-PEG600 3D printed films on viability of human fibroblast cells (10^5 cells/ml) at 24 and 48 hours respectively. Fig. 9 shows the MTT results of 3D printed films after 24 and 48 hours of incubation. After 24 hours, 97.38% of the human fibroblast cells were viable while more than 90% were viable after 48 hours. Based on the ISO guidelines for medical devices and biomaterials, for materials such as wound dressing to be accepted as biocompatible, the cell viability after exposure should be $\geq$ 70% (Moritz et al., 2014). The results clearly show that the CH-GE-PEG600 3D printed films are biocompatible with human fibroblast cells with cell viability values greater than 70%, and expected not to cause any skin irritation or interfere with cell proliferation. This is not surprising since CH is a known safe material approved for use in several biomedical and pharmaceutical formulations such as moist wound dressings (Patrulea et al., 2015). Zhang and co-authors (Zhang et al., 2008) and Ribeiro and co-authors (Ribeiro et al., 2009) investigated CH/PEG diacrylate films and CH hydrogels cytoxicity respectively and concluded that CH exerted no acute toxicity.

4. Conclusion

3D printing was employed for the preparation film based dressings comprising CH, GE and PEG for potential wound healing applications and facilitated the fabrication of wound dressing

scaffolds having control over geometry and interconnectivity. The GE crosslinked CH gels were deposited layer upon layer using jet dispenser to provide a fine 3D printed dressing. CH-GE-PEG600 3D printed films having the ratio of 1:1 polymer: plasticizer was selected due to their relatively high flexibility essential for easy application. Fourier transform infrared characterization of the 3D printed dressings showed inter molecular interaction between CH, GE and PEG confirming the crosslinking. *In vitro* mucoadhesion studies of CH-GE-PEG600 films showed the capability of the 3D printed film to adhere to the model mucosal surface. Further, swelling and in vitro drug release using FS as model drug showed that the crosslinked printed film was able to swell and release the model drug which is useful for managing wound exudate, maintain a moist environment whilst providing appropriate therapeutic drug doses within a reasonable time frame. Cytotoxicity assay (MTT) demonstrated that more than 90% of cells were viable after 48 hours which shows that the 3D printed CH-GE-PEG600 films are not toxic and therefore biocompatible with human skin and should not interfere with cell proliferation when applied to a wound. In conclusion, 3D printed CH-GE films seem to be promising dressing for potential chronic wound healing application. Future studies will involve more advanced wound healing characterization using active ingredients more specific to the wound healing process.

Declarations of interest: None

Acknowledgments: Authors are grateful to Mr Andrew Hurt for his help with scanning electron microscopy and X-ray diffraction analyses.

REFERENCES

Arteche P.M., Pérez-Álvarez, L., Cesteros Iturbe, L.C., Katime, I., 2013. Biodegradable chitosan nanogels crosslinked with genipin. Carbohydr. Polym. 94(2):836-842.

https://doi.org/10.1016/j.carbpol.2013.01.082.

Azevedo, E.P., Saldanha, T.D.P., Navarro, M.V.M., Medeiros, A.C., Ginani, M.F., Raffin, F.N., 2006. Mechanical properties and release studies of chitosan films impregnated with silver sulfadiazine. J. Appl. Polym. Sci. 102, 3462–3470. https://doi.org/10.1002/app.24537

Bhargavi CHS, Kumar ADA, K.N. and B.V., 2011. Ancient and Modern View of Wound Healing: Therapeutic Treatments. Research Journal of Pharmaceutical, Biological and Chemical Sciences. Res. J. Pharm. Biol. Chem. 2, 474–479.

Bhattarai, N., Ramay, H.R., Gunn, J., Matsen, F.A., Zhang, M., 2005. PEG-grafted chitosan as an injectable thermosensitive hydrogel for sustained protein release. J. Control. Release 103, 609–624. https://doi.org/10.1016/j.jconrel.2004.12.019

Blaeser, A., Duarte Campos, D.F., Weber, M., Neuss, S., Theek, B., Fischer, H., Jahnen-Dechent, W., 2013. Biofabrication Under Fluorocarbon: A Novel Freeform Fabrication Technique to Generate High Aspect Ratio Tissue-Engineered Constructs. Biores. Open Access 2, 374–384. https://doi.org/10.1089/biores.2013.0031

Boateng, J., Catanzano, O., 2015. Advanced therapeutic dressings for effective wound healing—a review. J. Pharm. Sci. 104, 3653–3680. https://doi.org/10.1002/jps.24610

Boateng, J.S., Ayensu, I., 2014. Preparation and characterization of laminated thiolated chitosan-based freeze-dried wafers for potential buccal delivery of macromolecules. Drug Dev. Ind. Pharm. 40, 611–618. https://doi.org/10.3109/03639045.2014.884126

Boateng, J.S., Matthews, K.H., Stevens, H.N.E., Eccleston, G.M., 2007. Wound healing dressings and drug delivery systems: A review. J. Pharm. Sci. 97, 2892–2923. https://doi.org/10.1002/jps.21210

Boateng, J.S., Stevens, H.N., Eccleston, G.M., Auffret, A.D., Humphrey, M.J., Matthews, K.H., 2009. Development and mechanical characterization of solvent-cast polymeric films as potential drug delivery systems to mucosal surfaces. Drug Dev. Ind. Pharm. 35, 986–996. https://doi.org/10.1080/03639040902744704

Bowler, P.G., Duerden, B.I., Armstrong, D.G., 2001. Wound microbiology and associated approaches to wound management. Clin. Microbiol. Rev. 14, 244-269. https://doi.org/10.1128/CMR.14.2.244-269.2001.

Chiono, V., Pulieri, E., Vozzi, G., Ciardelli, G., Ahluwalia, A., Giusti, P. 2008. Genipin-crosslinked chitosan/gelatin blends for biomedical applications. J. Mater. Sci.: Mater. Med. 19, 889-898. doi:10.1007/s10856-007-3212-5.

Cutting, K.F., 2010. Wound dressings : 21st century performance requirements. J. Wound Care 19, 4–9. https://doi.org/10.12968/jowc.2010.19.Sup1.48258.

Dean, D.M., Napolitano, A.P., Youssef, J., Morgan, J.R., 2007. Rods, tori, and honeycombs: the directed self-assembly of microtissues with prescribed microscale geometries. FASEB J. 21, 4005–4012. https://doi.org/10.1096/fj.07-8710com

Delgadillo-Armendariz, N.L., Rangel-Vazquez, N.A., Marquez-Brazon, E.A., Rojas-De Gascue, B., 2014. Interactions of chitosan/genipin hydrogels during drug delivery: A QSPR approach. Quim. Nova 37, 1503–1509. https://doi.org/10.5935/0100-4042.20140243

Desai, K.G.H., Park, H.J., 2005. Preparation and characterization of drug-loaded chitosan-tripolyphosphate microspheres by spray drying. Drug Dev. Res. 64, 114–128. https://doi.org/10.1002/ddr.10416

Dhivya, S., Padma, V. V., Santhini, E., 2015. Wound dressings – a review. BioMed. 5, 24–

28. doi: 10.7603/s40681-015-0022-9.

Ehrenreich, M., Ruszczak, Z., 2006. Tissue-engineered temporary wound coverings. Important options for the clinician. Acta Dermatov. APA. 15, 5-13.

Fan, K., Tang, J., Escandon, J., Kirsner, R.S., 2011. State of the Art in Topical Wound-Healing Products. Plast. Reconstr. Surg. 127, 44S–59S. https://doi.org/10.1097/PRS.0b013e3181fbe275

Hafezi, F., Kucukgul, C., Ozler, S. B. and Koc, B., 2016. Bioprinting: Application of Additive Manufacturing in Medicine, in: Amit Bandyopadhyay and Susmita Bose ed (Ed.), Additive Manufacturing.

Jones, J.E., Nelson, E.A., 2007. Skin grafting for venous leg ulcers. Cochrane Database Syst. Rev. CD001737. https://doi.org/http://dx.doi.org/10.1002/14651858.CD001737.pub3

Karbowiak, T., Hervet, H., Léger, L., Champion, D., Debeaufort, F., Voilley, A., 2006. Effect of plasticizers (water and glycerol) on the diffusion of a small molecule in iota-carrageenan biopolymer films for edible coating application. Biomacromol. 7, 2011–2019. https://doi.org/10.1021/bm060179r

Karki, S., Kim, H., Na, S.J., Shin, D., Jo, K., Lee, J., 2016. Thin films as an emerging platform for drug delivery. Asian J. Pharm. Sci. 11, 559–574. https://doi.org/10.1016/j.ajps.2016.05.004

Klein, M.P., Hackenhaar, C.R., Lorenzoni, A.S.G., Rodrigues, R.C., Costa, T.M.H., Ninow, J.L., Hertz, P.F., 2016. Chitosan crosslinked with genipin as support matrix for application in food process: Support characterization and β- d -galactosidase immobilization. Carbohydr. Polym. 137, 184–190. https://doi.org/10.1016/j.carbpol.2015.10.069

Lambert, J.B., Shurvell, H.F., Cooks, R.G., 1987. Introduction to Organic Spectroscopy. Introd. to Org. Spectrosc. 174–177. https://doi.org/10.1007/s11746-015-2722-4

Larjava, H., Salo, T., Haapasalmi, K., Kramer, R.H., Heino, J., 1993. Expression of integrins and basement membrane components by wound keratinocytes. J. Clin. Invest. 92, 1425–1435. https://doi.org/10.1172/JCI116719

Lee, K.Y., Mooney, D.J., 2012. Alginate: properties and biomedical applications. Prog. Polym. Sci. 37, 106–126. https://doi.org/10.1016/j.progpolymsci.2011.06.003

Leong, K.F., Cheah, C.M., Chua, C.K., 2003. Solid freeform fabrication of three-dimensional scaffolds for engineering replacement tissues and organs. Biomaterials 24, 2363–2378. https://doi.org/10.1016/S0142-9612(03)00030-9

Li, Q., Zhou, J., Zhang, L., 2009. Structure and properties of the nanocomposite films of chitosan reinforced with cellulose whiskers. J. Polym. Sci. Part B Polym. Phys. 47, 1069–1077. https://doi.org/10.1002/polb.21711

Liu, H., Adhikari, R., Guo, Q., Adhikari, B., 2013. Preparation and characterization of glycerol plasticized (high-amylose) starch-chitosan films. J. Food Eng. 116, 588–597. https://doi.org/10.1016/j.jfoodeng.2012.12.037

Liu, J., Chi, J., Wang, K., Liu, X., Liu, J., Gu, F., 2016. Full-thickness wound healing using 3D bioprinted gelatin-alginate scaffolds in mice: A histopathological study. Int. J. Clin. Exp. Pathol. 9, 11197–11205.

Liu, Y., Chen, W., Kim, H.-I., 2012. pH-responsive release behavior of genipin-crosslinked chitosan/poly(ethylene glycol) hydrogels. J. Appl. Polym. Sci. 125, E290–E298. https://doi.org/10.1002/app.36899

Meng, J., Lin, S., Xiong, X., 2017. Preparation of breathable and superhydrophobic coating

film via spray coating in combination with vapor-induced phase separation. Prog. Org. Coatings 107, 29–36. https://doi.org/10.1016/j.porgcoat.2017.03.004

Mi, F.L., Sung, H.W., Shyu, S.S., 2001. Release of indomethacin from a novel chitosan microsphere prepared by a naturally occurring crosslinker: Examination of crosslinking and polycation-anionic drug interaction. J. Appl. Polym. Sci. 81, 1700–1711. https://doi.org/10.1002/app.1602

Morales, J.O., McConville, J.T., 2011. Manufacture and characterization of mucoadhesive buccal films. Eur. J. Pharm. Biopharm. 77, 187-199. https://doi.org/10.1016/j.ejpb.2010.11.023

Morgan, D., 2002. Wounds: what dressings should a formulary include. Hosp Pharm 9, 261–266.

Moritz, S., Wiegand, C., Wesarg, F., Hessler, N., Müller, F.A., Kralisch, D., Hipler, U.C., Fischer, D., 2014. Active wound dressings based on bacterial nanocellulose as drug delivery system for octenidine. Int. J. Pharm. 471, 45–55. https://doi.org/10.1016/j.ijpharm.2014.04.062

Murphy, S. V, Atala, A., 2014. 3D bioprinting of tissues and organs. Nat. Biotechnol. 32, 773-785. https://doi.org/10.1038/nbt.2958

Muzzarelli, R. A., 2009. Genipin-crosslinked chitosan hydrogels as biomedical and pharmaceutical aids. Carbohydr. Polym. 77, 1-9. https://doi.org/10.1016/j.carbpol.2009.01.016

Muzzarelli, R.A.A., El Mehtedi, M., Bottegoni, C., Aquili, A., Gigante, A., 2015. Genipin-crosslinked chitosan gels and scaffolds for tissue engineering and regeneration of cartilage and bone. Mar. Drugs. 13, 7314-7338. https://doi.org/10.3390/md13127068

Niesman, M.R., Khoobehi, B., Peyman, G.A., 1992. Encapsulation of sodium fluorescein for dye release studies. Investig. Ophthalmol. Vis. Sci. https://doi.org/10.1021/jo00296a062

Nunes, C., Maricato, É., Cunha, Â., Rocha, M.A.M., Santos, S., Ferreira, P., Silva, M.A., Rodrigues, A., Amado, O., Coimbra, J., Silva, D., Moreira, A., Mendo, S., Lopes Da Silva, J.A., Pereira, E., Rocha, S.M., Coimbra, M.A., 2016. Chitosan-genipin film, a sustainable methodology for wine preservation. Green Chem. 18, 5331–5341. https://doi.org/10.1039/c6gc01621a

Ousey, K., Gillibrand, W., Stephenson, J., 2011. Understanding and preventing wound blistering. Wounds UK. 7, 50-56.

Patrulea, V., Ostafe, V., Borchard, G., Jordan, O., 2015. Chitosan as a starting material for wound healing applications. Eur. J. Pharm. Biopharm. 97, 417-426. https://doi.org/10.1016/j.ejpb.2015.08.004

Pham, V.H., Cuong, T.V., Hur, S.H., Shin, E.W., Kim, J.S., Chung, J.S., Kim, E.J., 2010. Fast and simple fabrication of a large transparent chemically-converted graphene film by spray-coating. Carbon N. Y. 48, 1945–1951. https://doi.org/10.1016/j.carbon.2010.01.062

Ribeiro, M.P., Espiga, A., Silva, D., Baptista, P., Henriques, J., Ferreira, C., Silva, J.C., Borges, J.P., Pires, E., Chaves, P., Correia, I.J., 2009. Development of a new chitosan hydrogel for wound dressing. Wound Repair Regen. 17, 817–824. https://doi.org/10.1111/j.1524-475X.2009.00538.x

Roy, S.K., Prabhakar, B., 2010. Bioadhesive polymeric platforms for transmucosal drug delivery systems - A review. Trop. J. Pharm. Res. 9, 91-104. https://doi.org/10.4314/tjpr.v9i1.52043

Schreml, S., Szeimies, R.M., Prantl, L., Karrer, S., Landthaler, M., Babilas, P., 2010. Oxygen in acute and chronic wound healing. Br. J. Dermatol. 163, 257-268. https://doi.org/10.1111/j.1365-2133.2010.09804.x

Scoutaris, N., Nion, A., Hurt, A., Douroumis, D., 2016. Jet dispensing as a high throughput method for rapid screening and manufacturing of cocrystals. CrystEngComm 18, 5079–5082. https://doi.org/10.1039/c6ce00664g

Singer, A.J., Clark, R.A.F., 1999. Cutaneous Wound Healing. N. Engl. J. Med. 341, 738–746. https://doi.org/10.1056/NEJM199909023411006

Sussman, G., 2010. Understanding film dressings. Wounds Int. 1, 23–25. https://doi.org/10.1111/j.1742-481X.2011.00923.x/abstract

Suyatma, N.E., Tighzert, L., Copinet, A., Coma, V., 2005. Effects of hydrophilic plasticizers on mechanical, thermal, and surface properties of chitosan films. J. Agric. Food Chem. 53, 3950–3957. https://doi.org/10.1021/jf048790+

Szymańska, E., Winnicka, K., 2015. Stability of chitosan - A challenge for pharmaceutical and biomedical applications. Mar. Drugs. 13, 1819-1846. https://doi.org/10.3390/md13041819

Tanaka, M., Iwata, K., Sanguandeekul, R., Handa, A., Ishizaki, S., 2001. Influence of plasticizers on the properties of edible films prepared from fish water-soluble proteins. Fish. Sci. 67, 346–351. https://doi.org/10.1046/j.1444-2906.2001.00237.x

Tong, C., Hao, H., Xia, L., Liu, J., Ti, D., Dong, L., Hou, Q., Song, H., Liu, H., Zhao, Y., Fu, X., Han, W., 2016. Hypoxia pretreatment of bone marrow - Derived mesenchymal stem cells seeded in a collagen-chitosan sponge scaffold promotes skin wound healing in diabetic rats with hindlimb ischemia. Wound Repair Regen. 24, 45–56.

https://doi.org/10.1111/wrr.12369

Vieira, M.G.A., Da Silva, M.A., Dos Santos, L.O., Beppu, M.M., 2011. Natural-based plasticizers and biopolymer films: A review. Eur. Polym. J. 47, 254-263. https://doi.org/10.1016/j.eurpolymj.2010.12.011

Winotapun, W., Opanasopit, P., Ngawhirunpat, T., Rojanarata, T., 2013. One-enzyme catalyzed simultaneous plant cell disruption and conversion of released glycoside to aglycone combined with in situ product separation as green one-pot production of genipin from gardenia fruit. Enzyme Microb. Technol. 53, 92-96. https://doi.org/10.1016/j.enzmictec.2013.05.001

Wittaya-Areekul, S., Prahsarn, C., 2006. Development and in vitro evaluation of chitosan-polysaccharides composite wound dressings. Int. J. Pharm. 313, 123–128. https://doi.org/10.1016/j.ijpharm.2006.01.027

Yadav, V.K., Gupta, A.B., Kumar, R., Yadav, J.S., Kumar, B., 2010. Mucoadhesive polymers: means of improving the mucoadhesive properties of drug delivery system. J. Chem. Pharm. Res. 2, 418-432.

Yu, T., Andrews, G.P., Jones, D.S., 2014. Mucoadhesion and characterization of mucoadhesive properties, in: Mucosal Delivery of Biopharmaceuticals: Biology, Challenges and Strategies. pp. 35–58. https://doi.org/10.1007/978-1-4614-9524-6_2

Zhang, T., Yan, K.C., Ouyang, L., Sun, W., 2013. Mechanical characterization of bioprinted in vitro soft tissue models. Biofabrication 5, 045010 (10 pages)

https://doi.org/10.1088/1758-5082/5/4/045010

Zhang, X., Yang, D., Nie, J., 2008. Chitosan/polyethylene glycol diacrylate films as potential wound dressing material. Int. J. Biol. Macromol. 43, 456–462.

https://doi.org/10.1016/j.ijbiomac.2008.08.010

Zhang, Y., Yu, Y.F., Shi, X.X., Zhao, S.C., Chen, A.B., Huang, D.W., Niu, D.J., Qin, Z., 2013. Study on the preparation of genipin crosslinked chitosan microspheres of resveratrol and in vitro release. J. Polym. Res. 20, 1-10. https://doi.org/10.1007/s10965-013-0175-8

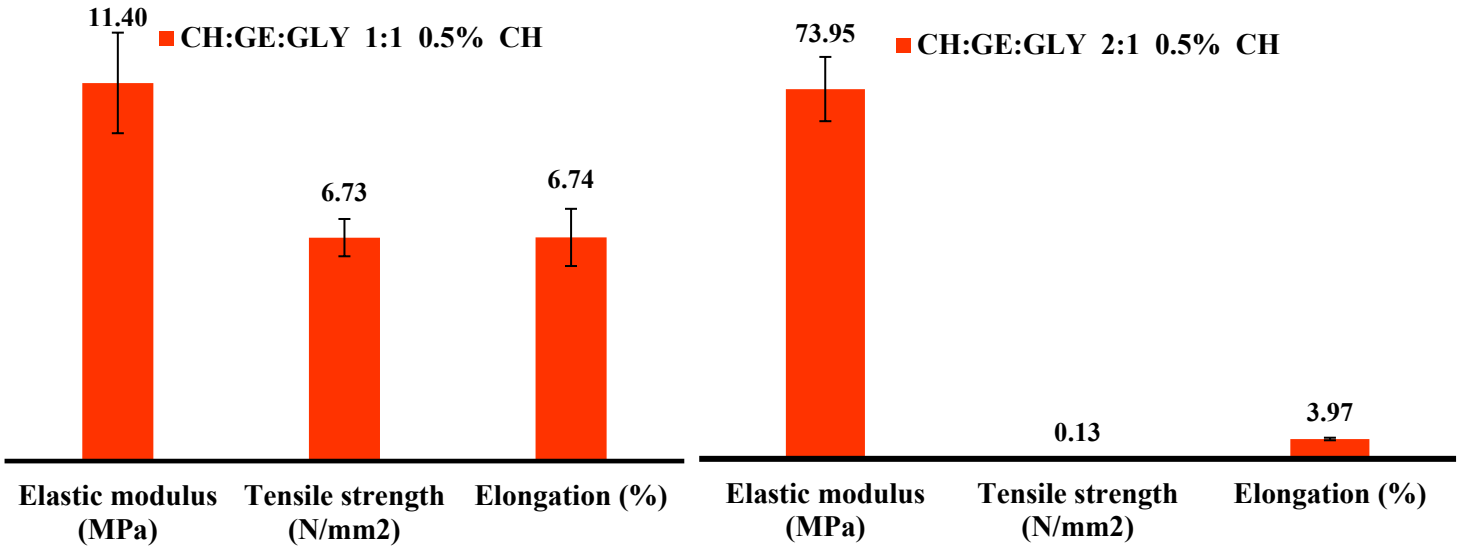

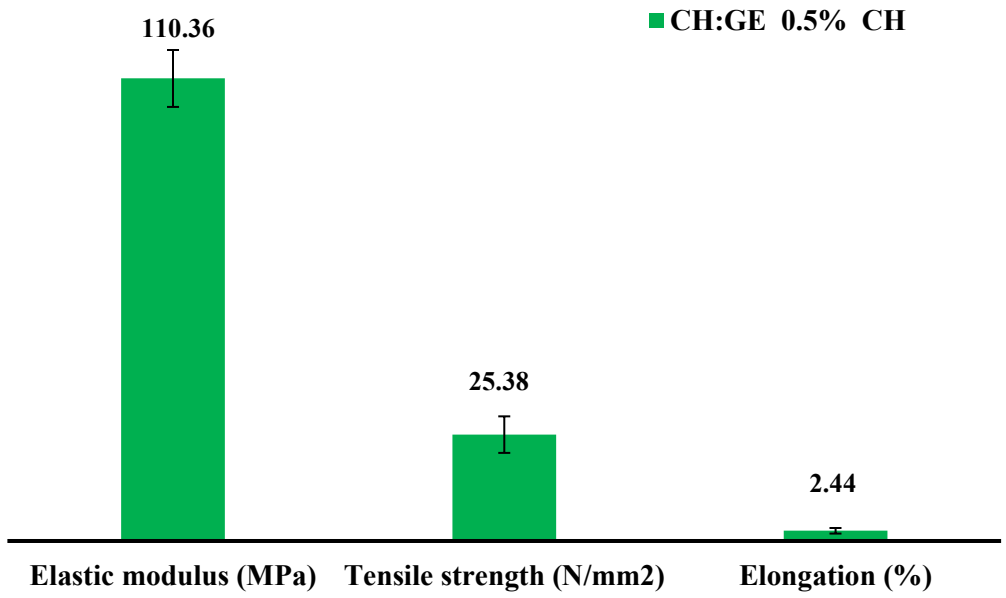

Figure 1 Elastic modulus, tensile strength and elongation at break for 3D printed CH-GE, CH-GE-GLY films (n = 3, ± SD)

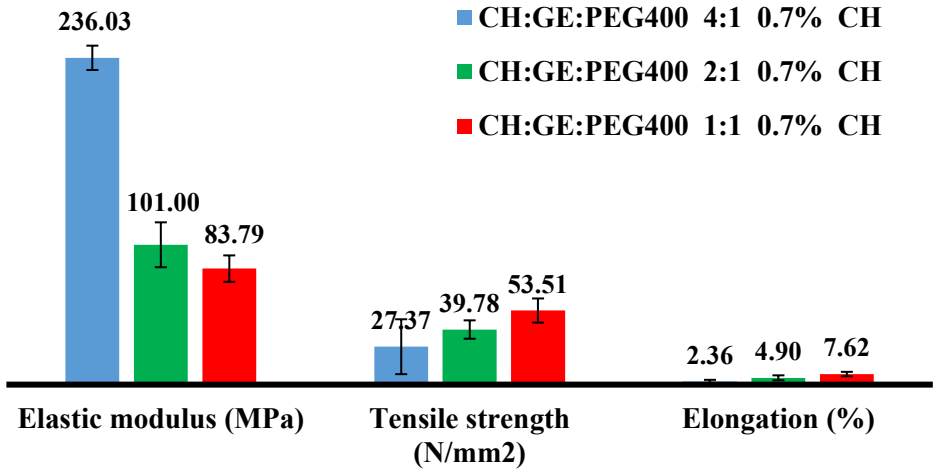
236.03
101.00
83.79
27.37
39.78
53.51
2.36
4.90
7.62
CH:GE:PEG400 4:1 0.7% CH
CH:GE:PEG400 2:1 0.7% CH
CH:GE:PEG400 1:1 0.7% CH
Elastic modulus (MPa)
Tensile strength (N/mm2)
Elongation (%)

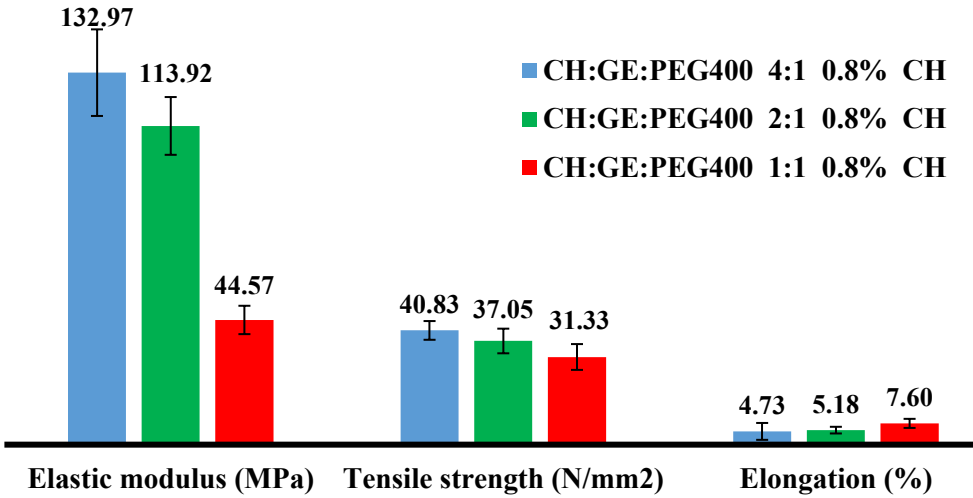
132.97
113.92
44.57
40.83
37.05
31.33
4.73
5.18
7.60
CH:GE:PEG400 4:1 0.8% CH
CH:GE:PEG400 2:1 0.8% CH
CH:GE:PEG400 1:1 0.8% CH
Elastic modulus (MPa)
Tensile strength (N/mm2)
Elongation (%)

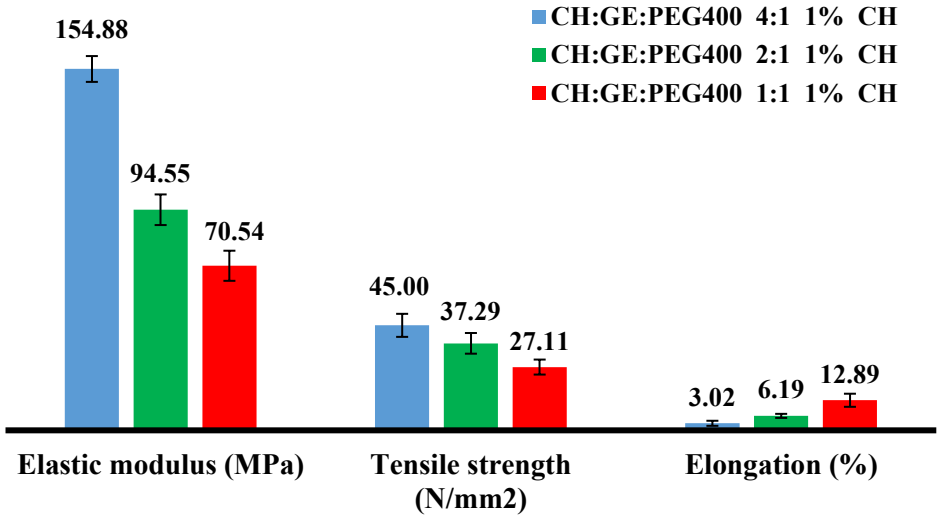
154.88
94.55
70.54
45.00
37.29
27.11
3.02
6.19
12.89
CH:GE:PEG400 4:1 1% CH
CH:GE:PEG400 2:1 1% CH
CH:GE:PEG400 1:1 1% CH
Elastic modulus (MPa)
Tensile strength (N/mm2)
Elongation (%)

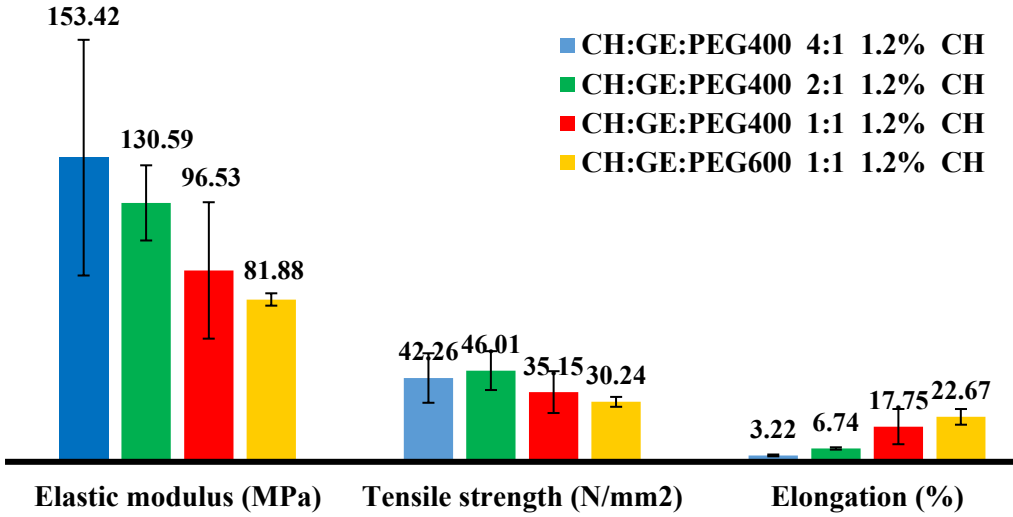
153.42
130.59
96.53
81.88
42.26
46.01
35.15
30.24
3.22
6.74
17.75
22.67
CH:GE:PEG400 4:1 1.2% CH
CH:GE:PEG400 2:1 1.2% CH
CH:GE:PEG400 1:1 1.2% CH
CH:GE:PEG600 1:1 1.2% CH
Elastic modulus (MPa)
Tensile strength (N/mm2)
Elongation (%)

ak)

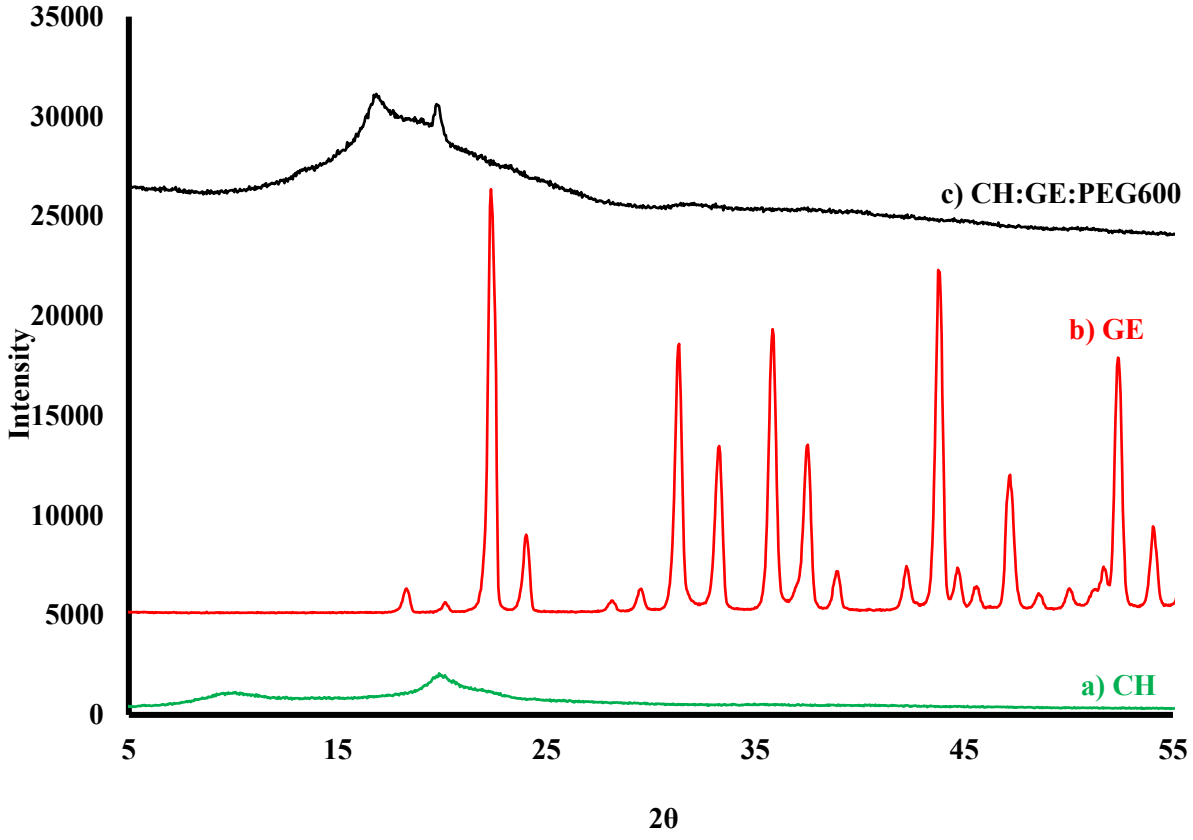

Figure 3 X-ray diffractograms of a) pure CH, b) pure GE, and c) 3D printed CH-GE-PEG600 films

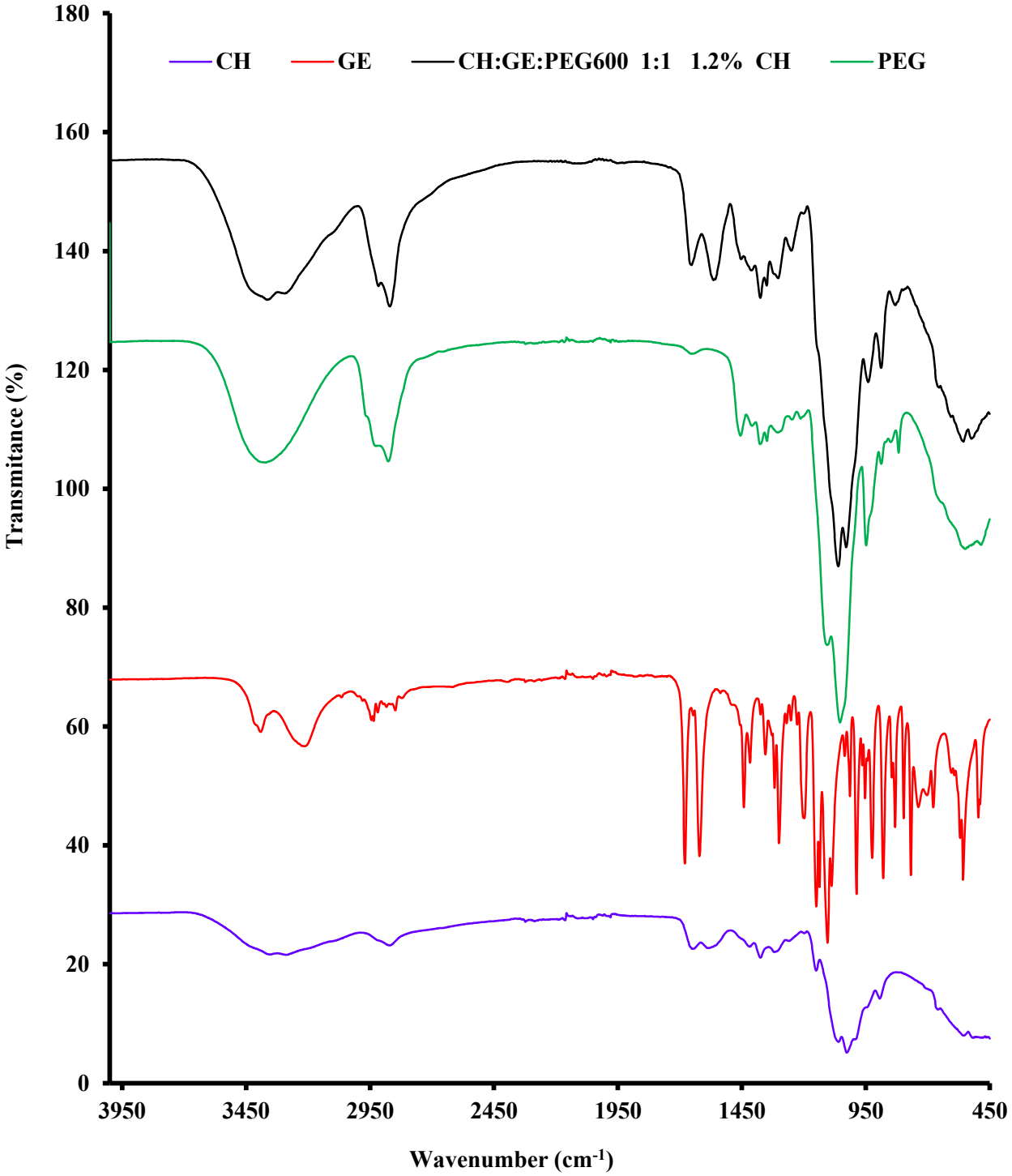

Figure 4 FTIR spectra of pure starting materials (CH, GE, PEG) and CH-GE-PEG600 3D printed film

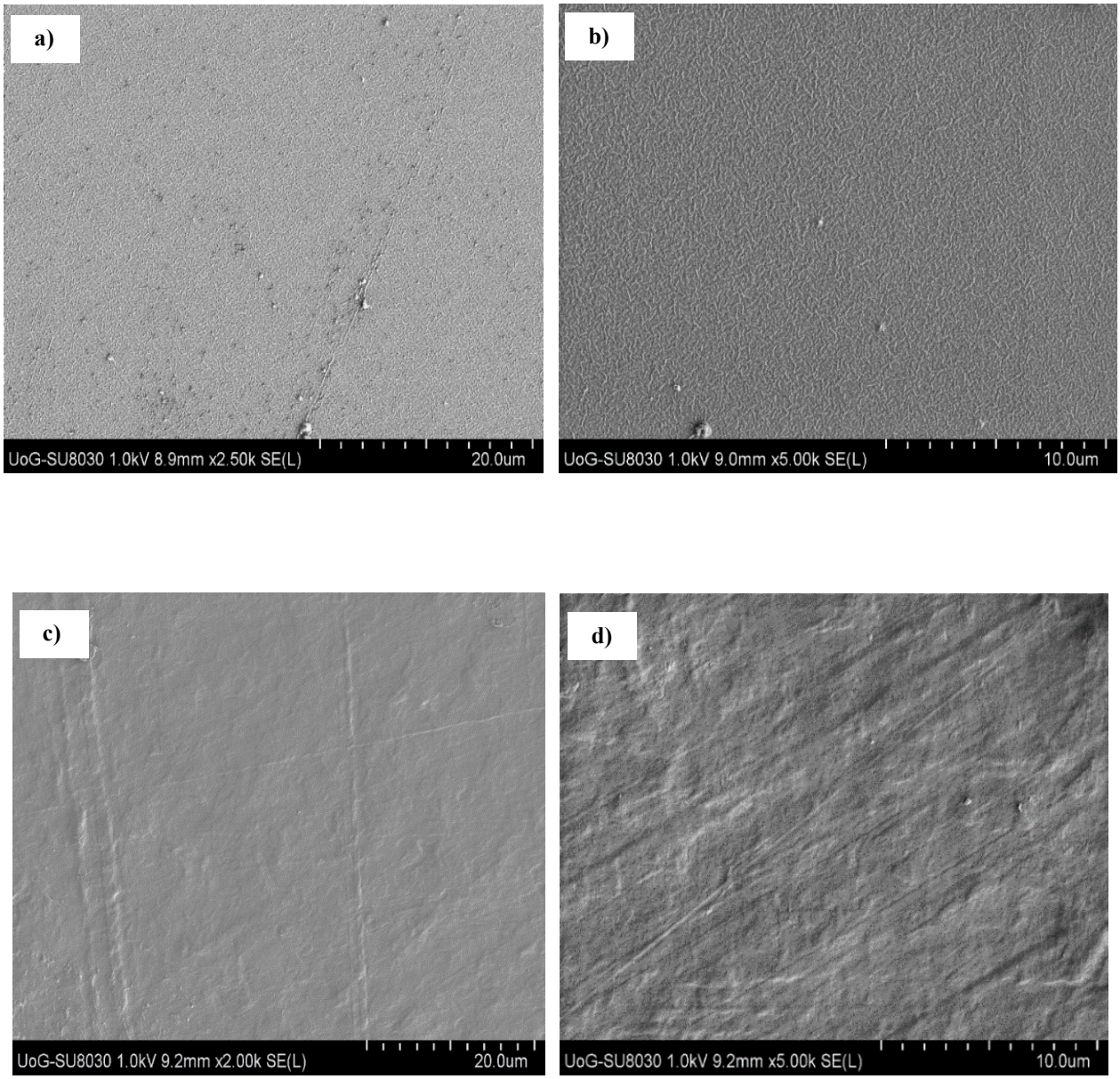

Figure 5 CH-GE and CH-GE-PEG600 3D printed film at magnifications of a) 40, b) 250, c) 2000 and d) 5000

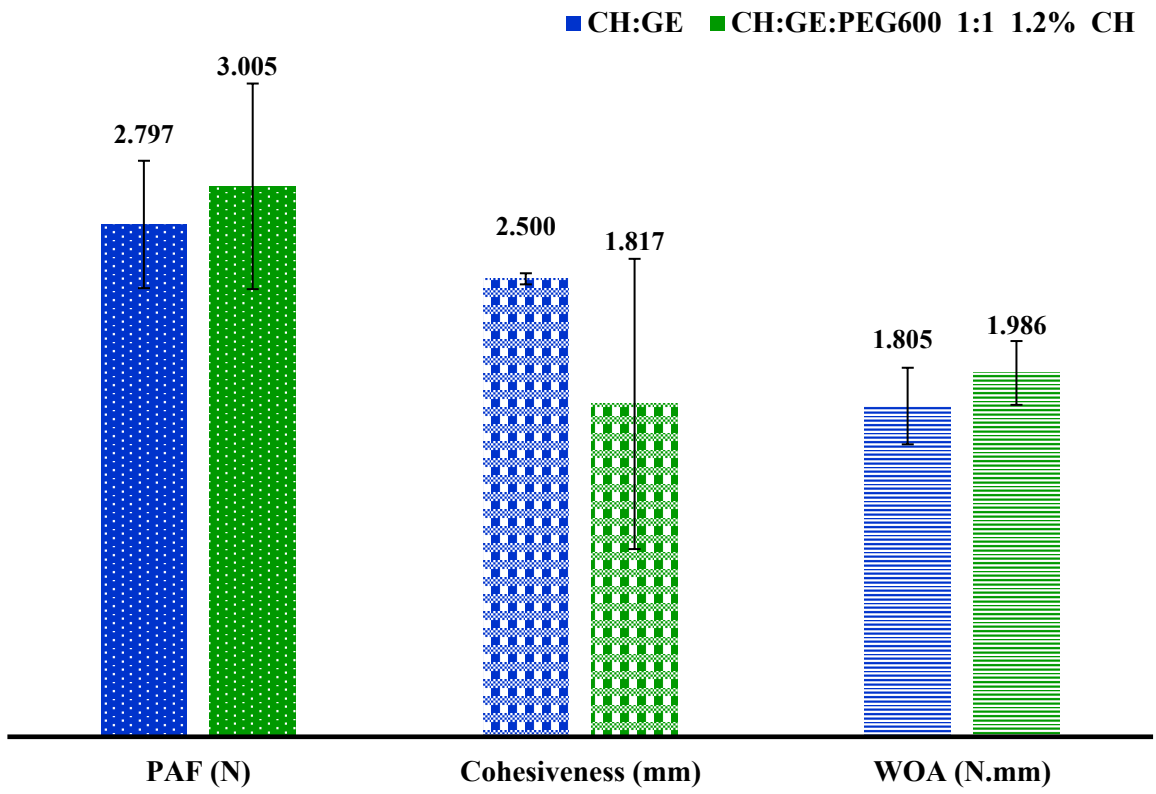

Figure 6. Mucoadhesion profiles of CH-GE and CH-GE-PEG600 3D printed films (n = 3, ± SD)

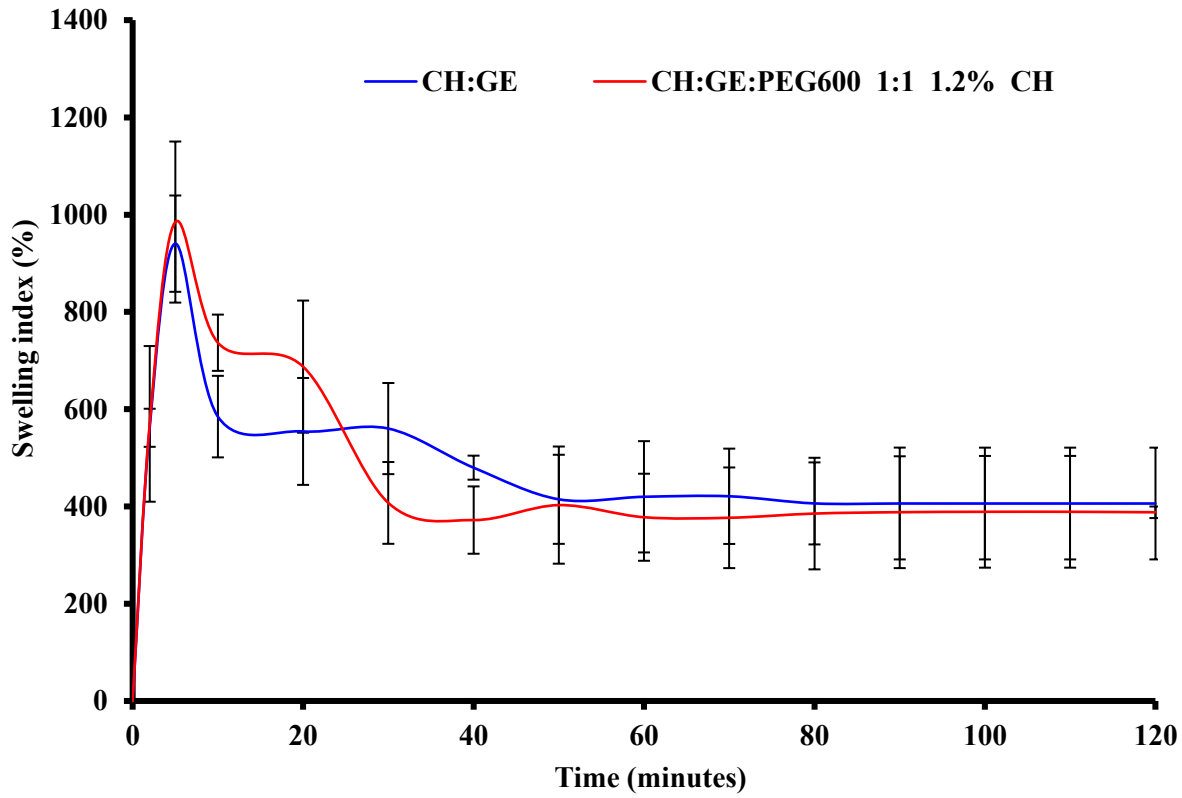

Figure 7 Swelling profiles showing the change in the % swelling index with time of CH-GE and CH-GE-PEG600 3D printed films (*n*=3, ±SD)

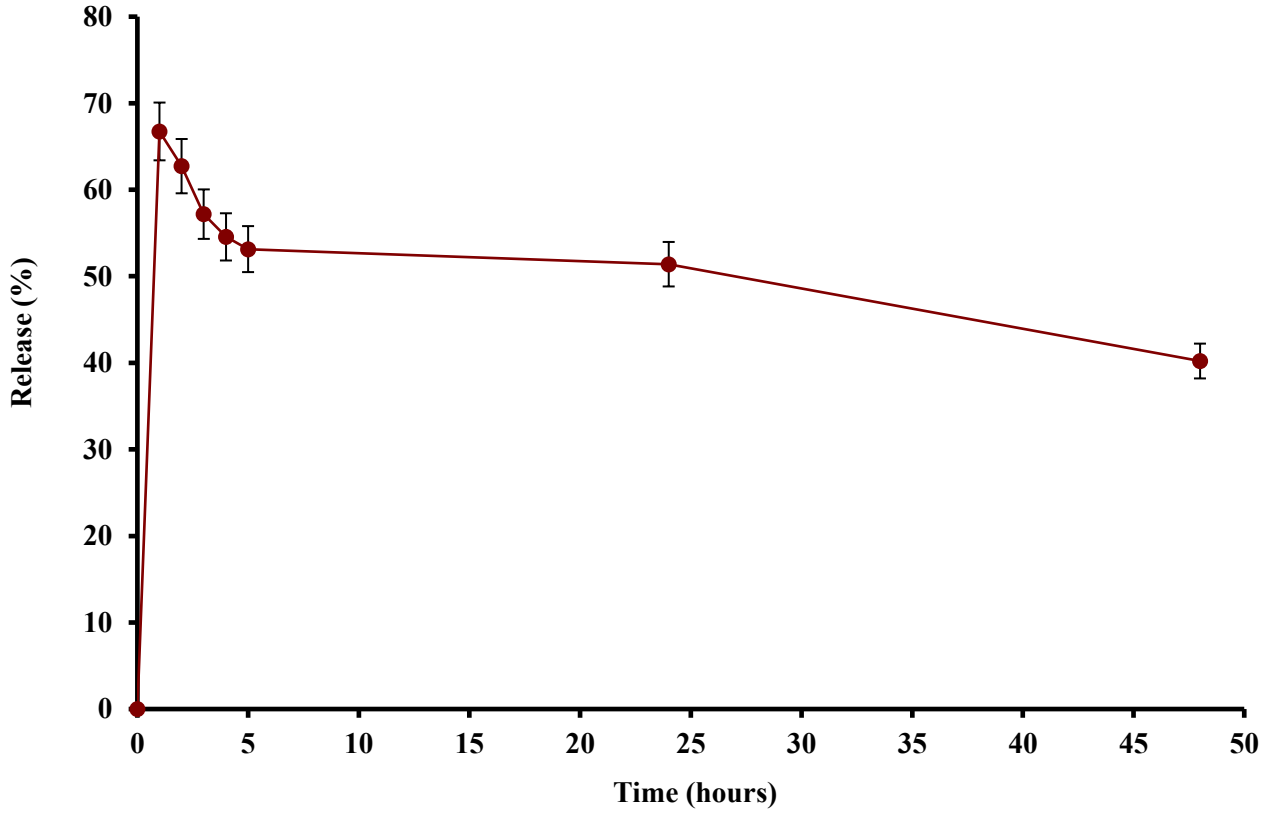

Figure 8 Drug dissolution profile of FS loaded CH-GE-FS-PEG600 3D printed films (*n*=3, ±SD) in PBS at pH 7.4

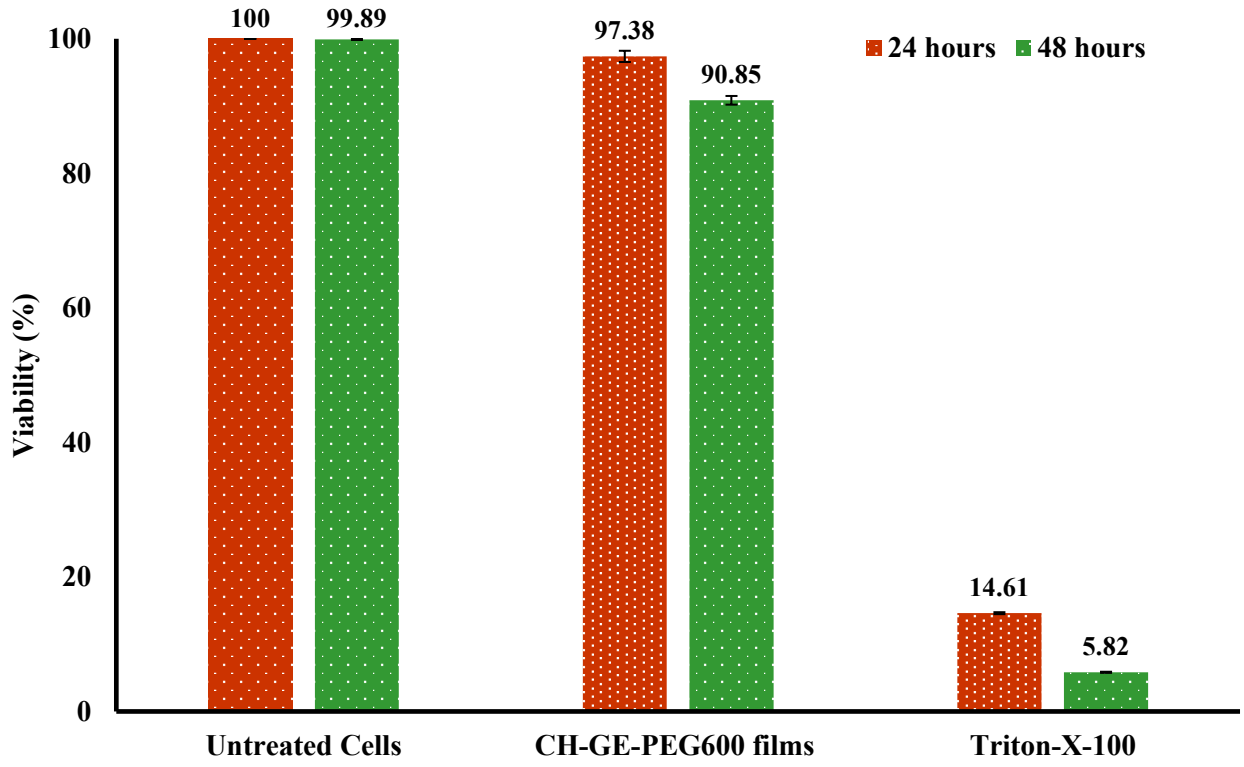

Figure 9 Cytotoxicity (MTT) analysis of the CH-GE-PEG600 3D printed films with untreated cells as negative control and Triton-X -100 as toxic positive control (n=3, ±SD)